Mechanism of Resistance Microwelding of Crossed Fine Nickel Wires

S. FUKUMOTO and Y. ZHOU

Resistance microwelding of fine crossed nickel wires is of increasing industrial importance for electrical connections in downsized electronic and medical devices, but the understanding of the process is very limited. A study has, therefore, been performed to clarify the basic joining mechanisms, in which the effects of main process parameters (welding current and force and weld time) were investigated by detailed mechanical testing and metallurgical examinations. A bonding mechanism with main process stages (wire cold collapse, surface melting, molten-phase squeeze-out and, solid-state bonding) was proposed. A new technique has also been developed to optimize the process by initiating the welding current well before the electrode force has reached its full nominal value.

I. INTRODUCTION

RESISTANCE cross-wire welding is one of the electric-resistance welding processes, in which two wires are joined to each other, usually at a right angle, by resistance heating under the effect of electrode force.[1] At a large or "regular" scale, cross-wire welded products (mainly of steels) include such items as stove and refrigerator racks, lamp shades, baskets, fencing, concrete reinforcing, *etc*.[1] At a small or microscale (usually with a wire diameter less than 0.2 to 0.5 mm), resistance cross-wire microwelding is commonly used in electronics and instrument components, mainly for electrical interconnections.[2,3] This latter area of resistance cross-wire welding is becoming increasingly important because of the rapid downsizing of manufactured products.

In resistance welding in general,[1] the heat required to form a joint between metals is generated by the resistance to the flow of electric current through the workpieces and can be mathematically described by

$$Q = I^2Rt \qquad [1]$$

where Q is the heat generation, I is the welding current, R is the resistance, and t is the duration of the current application (weld time). The resistance includes contact resistance at the electrode/workpiece and workpiece/workpiece interfaces and bulk resistance of the base materials.[4] Among these resistance components, the workpiece/workpiece contact resistance, which is influenced mainly by material properties (such as hardness and resistivity), surface characteristics (such as cleanliness and roughness), and electrode force, may be the most important factor affecting the process.[1,5,6] This is especially true in resistance microwelding because of the relatively low values of welding current, electrode force, and resistivities of nonferrous workpieces.[4,7]

It is generally considered that, in resistance cross-wire welding, "set down," an indication of the extent to which the wires are compressed into each other, can be used to evaluate joint strength.[1] For example, Moravskii *et al*.,[8] in an investigation of resistance cross-wire microwelding of various fine wires using a capacitor-discharge power supply, found that 30 to 35 pct setdown produced good joint quality, while Stroev *et al*.[3] observed an optimum setdown of 30 to 50 pct in a similar investigation, but on nickel lead-outs of 0.2 mm in diameter. It has been shown[2,3] that inadequate heat generation resulted in weak bonding with a low setdown, while weld-metal expulsion took place when the heat generation was too high, resulting a very high setdown but a low joint strength. When the joint was of high quality, the bond interface between the welded wires disappeared and the joint fractured through the heat-affected zone (HAZ).[2,3] However, those investigations were mainly concerned with equipment development and process optimization,[1–3,8] and there is, in general, a lack of detailed research work published on resistance cross-wire welding, especially on bonding mechanisms, at both large and small scales.

The objective of this work was to study the weldability and mechanism of resistance microwelding of crossed fine nickel wires by carrying out closely controlled and monitored welding trials and, subsequently, detailed mechanical testing and metallurgical examination.

II. EXPERIMENTAL

A 99 pct commercially pure nickel (Ni 200) drawn wire of 0.4 mm in diameter was used in this study. The principal impurities in the wire as reported by the manufacturer are shown in Table I. The wire was cleaned with acetone prior to welding, but traces of sulfur, manganese, and, maybe, silicon were present on or near the wire surfaces (Figures 1 and 2). These might be due to the inclusions (Figure 1(b)) and/or residues of lubricants (generally containing MoS, for example) used in the wire-drawing process.

The angle between the axes of crossed wires was about 90 deg (Figure 3). The resistance microwelding system consisted of a Unitek PM7/208 alternating-current (a.c.) controller (at 60 Hz), a Unitek X16/230 a.c. transformer, and a Unitek 80A/115 weld head (air activated). Flat-ended, round RWMA class II (Cu-Cr) electrodes, 3.2 mm in diameter, were used. Variables in the experimental matrix included welding current, welding

S. FUKUMOTO, Research Associate, is with the Graduate School, Himeji Institute of Technology, Himeji, Hyogo, Japan 671-2201. Y. ZHOU, Canada Research Chair in Microjoining (www.chairs.gc.ca), is with the Department of Mechanical Engineering, University of Waterloo, Waterloo, ON, Canada N2L 3G1. Contact e-mail: nzhou@uwaterloo.ca

Manuscript submitted February 9, 2004.

force, and weld time, since these are among the principal parameters that affect heat generation. The welding system was programmed to first apply air pressure to the electrode-force mechanism and then to initiate the welding current when the electrode force reached a specific level (*i.e.*, the firing force, which was normally set to be approximately 90 to 97 pct of the welding force). The current was altered by voltage (*i.e.*, by changing secondary tap settings) and conduction angle (*i.e.*, by switching off the current for a portion of each cycle) in the welding-current controller, and the root-mean-square value was measured. Five nominally identical samples were made at each condition. The breaking force of the joints was evaluated as an indication of joint strength by tensile-shear testing using a Quad Romulus IV universal mechanical tester. Wire deformation after welding was evaluated by the parameter of setdown, which was calculated by the thickness of the joint assembly before and after welding:

$$\text{Setdown} = \frac{A - B}{A} \times 100 \text{ (pct)} \quad [2]$$

where A and B are defined in Figure 3(b). Cross sections and fractured surfaces of the joints were examined by an optical

Table I. Chemical Impurities in Nickel Wire (in ppm)

Cu	Co	Fe	Mg	Mn	Si	Ti	C	S
<100	400	100	650	900	1000	<100	320	<10

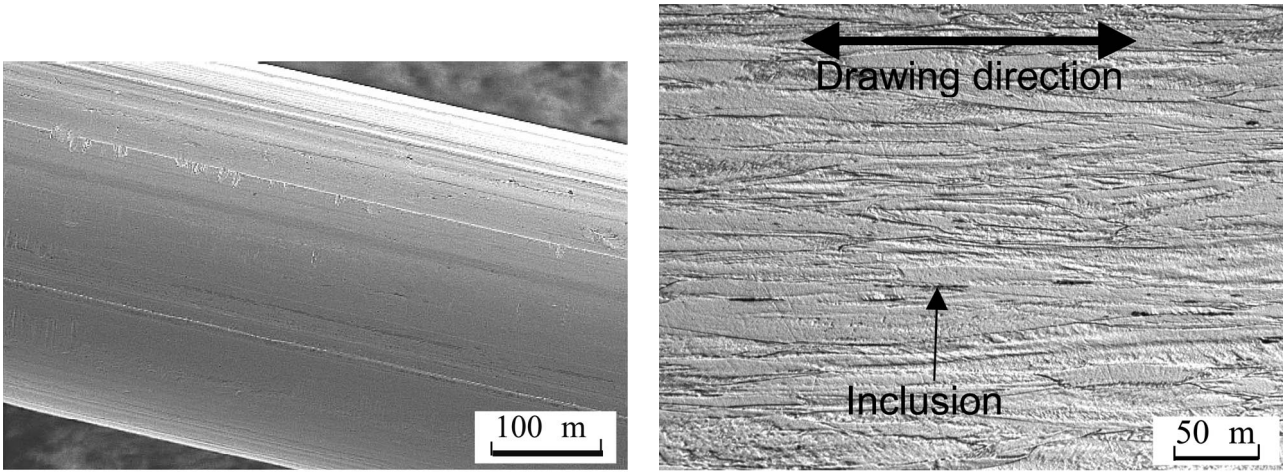

Fig. 1—As-received nickel wire: (*a*) wire surface and (*b*) cross section of wire.

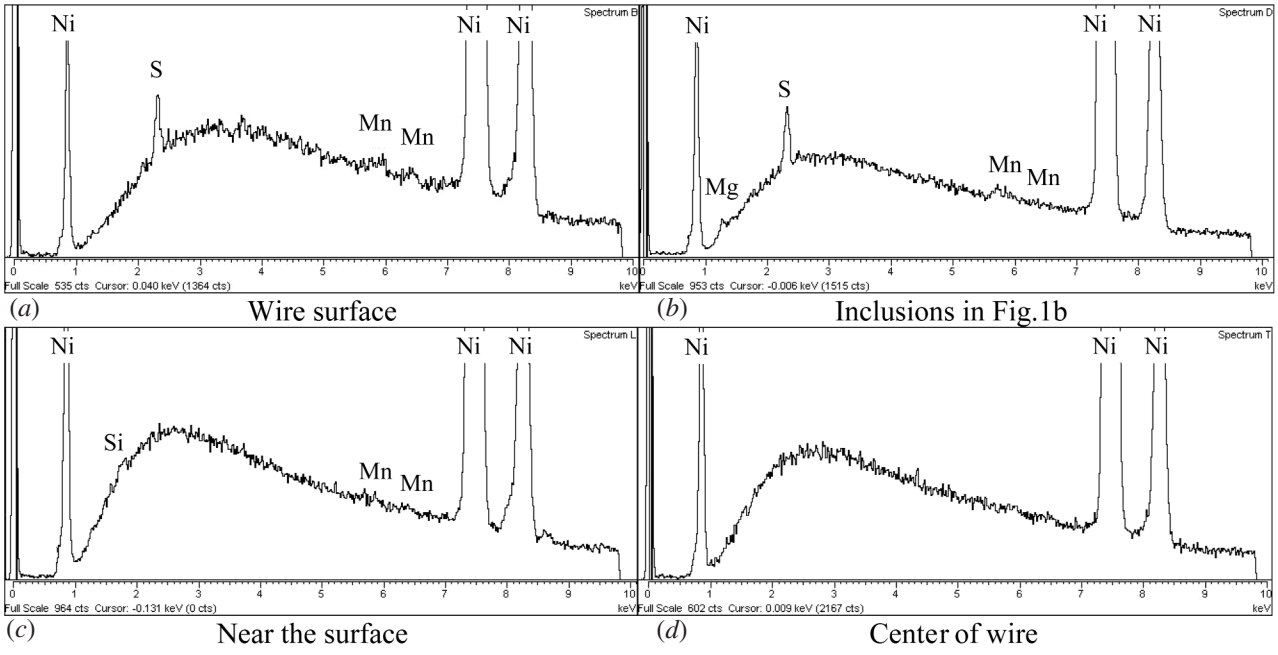

Fig. 2—EDX analyses of as-received wire: (*a*) wire surface, (*b*) inclusions in Fig. 1(b), (*c*) near the surface, and (*d*) center of wire.

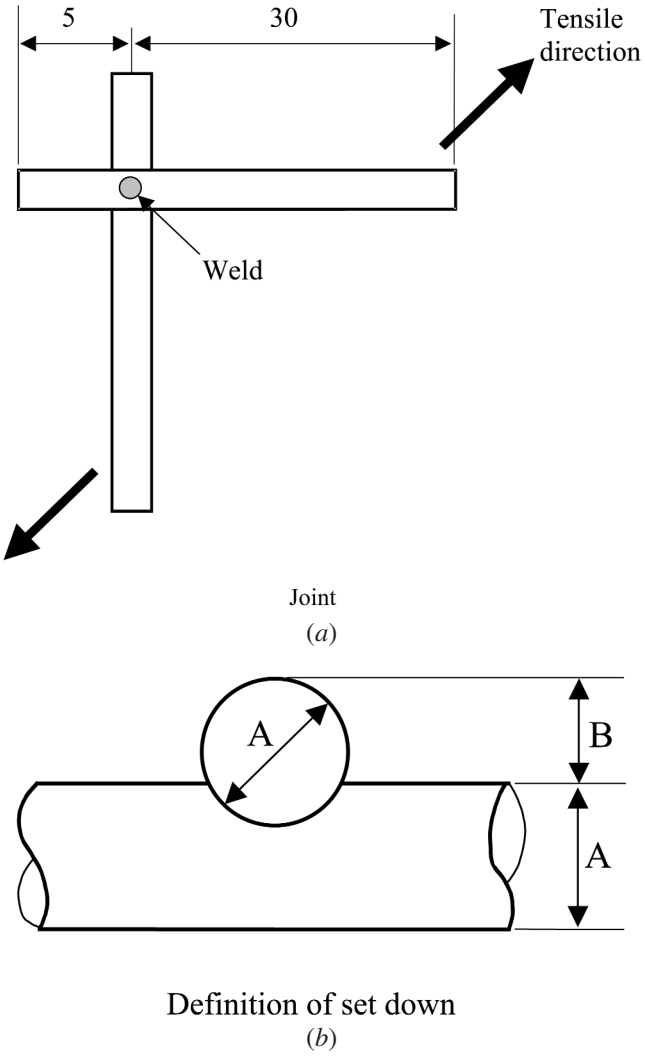

Fig. 3—Schematic illustrations of cross-wire joint: (*a*) joint and (*b*) definition of setdown.

microscope and/or scanning electron microscope (SEM) with energy-dispersive X-ray (EDX) spectroscopy. Metallographic samples were prepared by etching for 30 seconds with a solution containing 13 g $CuSO_4$, 60 mL HCl, 3 mL HF, 3 mL HNO_3, and 150 mL water after 1 μm diamond polishing. The microscale Vickers hardness was measured on cross sections of joints under the load of 15 g. The static contact resistance between wires was measured by the crossed-rod, voltmeter-ammeter method[9] under the welding force without current.

III. RESULTS

A. *Effects of Welding Current*

Typical joint cross sections made with various welding currents are shown in Figures 4 and 5. The wires were squashed and penetrated into each other to varying degrees, and the HAZ, with a recrystallized microstructure, was obvious on etched samples. Both the grain size and extent of the HAZ grew as the current increased. Although the bond interface could be identified because of the preferential etching in joints made with lower welding currents, the line eventually disappeared, with new grains growing across the bond interface as the recrystallization progressed (Figures 4(d) and 5(b)). Some annealing twins were formed even near the bond interface at higher welding currents (Figure 5(c)). Expelled material (weld flash) was also observed at relatively high welding currents, as shown in Figures 4(c) and (d) and 5(d), and this appeared to be a result of liquid phase squeezed out from the bond interface (as discussed in detail later). When the current was too high, melting of bulk material occurred, especially in the electrode-wire contact area, as indicated by the solidified columnar grains (Figure 4(e)), and severe electrode sticking to the wire and weld metal expulsion were observed.

Figure 6 shows the effects of welding current on the joint breaking force (as an indication of joint strength) and setdown. The setdown increased monotonically as the current increased, but the breaking force increased first and subsequently decreased after further increasing the current. Corresponding to the change in welding current, the fracture mode also changed from interfacial shear fracture to tensile fracture in the HAZ. This characteristic behavior of the breaking force is believed to result from competition between the improvement of interfacial bonding (determined by both the bonded area and interfacial strength) and the local softening of the wire in the HAZ (resulting from recrystallization). When the interfacial bonding was weak, the joint failed through bond interface. The increase in bonded area (as indicated by the increased setdown) and/or interfacial strength (as indicated by the disappearing of the bond interface in Figure 4) increased the load required to fracture the bond. However, with the increasing welding current, the HAZ near the bond interface became the weaker region of the joint because of recrystallization of the originally cold-drawn microstructure, and the fracture mode switched to the HAZ failure. A further increase of welding current resulted in a reduction in joint breaking force as the recrystallization continued to progress. The vickers hardness of the fully recrystallized HAZ and as-received wire were approximately HV140 and 180, respectively, which means that additional strength of the wire itself introduced by cold drawing during wire manufacture was lost due to the recrystallization. It should be pointed out that even when the joint breaking force continued to decrease, the interfacial strength would continue to increase as the bond interface was disappearing (Figure 4(d)).

The observation that joint breaking force increased before reaching its maximum with an increase of setdown is consistent with previous work,[1–3,8] but the optimum setdown in this work, at about 80 to 90 pct, was much higher than that reported in the literature.[3,8] This may be due to many differences in experimental conditions (such as wire compositions and properties and welding power supplies).

B. *Effects of Weld Time*

The effects of weld time on joint microstructure, breaking force, and wire setdown are shown in Figures 7 and 8. The microstructures showed that the peak temperature was not affected much by the weld time, because the HAZ area and grain size did not show any significant evolution against the weld time (Figure 7), compared to the changes caused by the current (Figure 4). Even after the first cycle, the recrystallized microstructure was almost fully developed near the bond interface, similar to specimens with as much as 12 cycles of

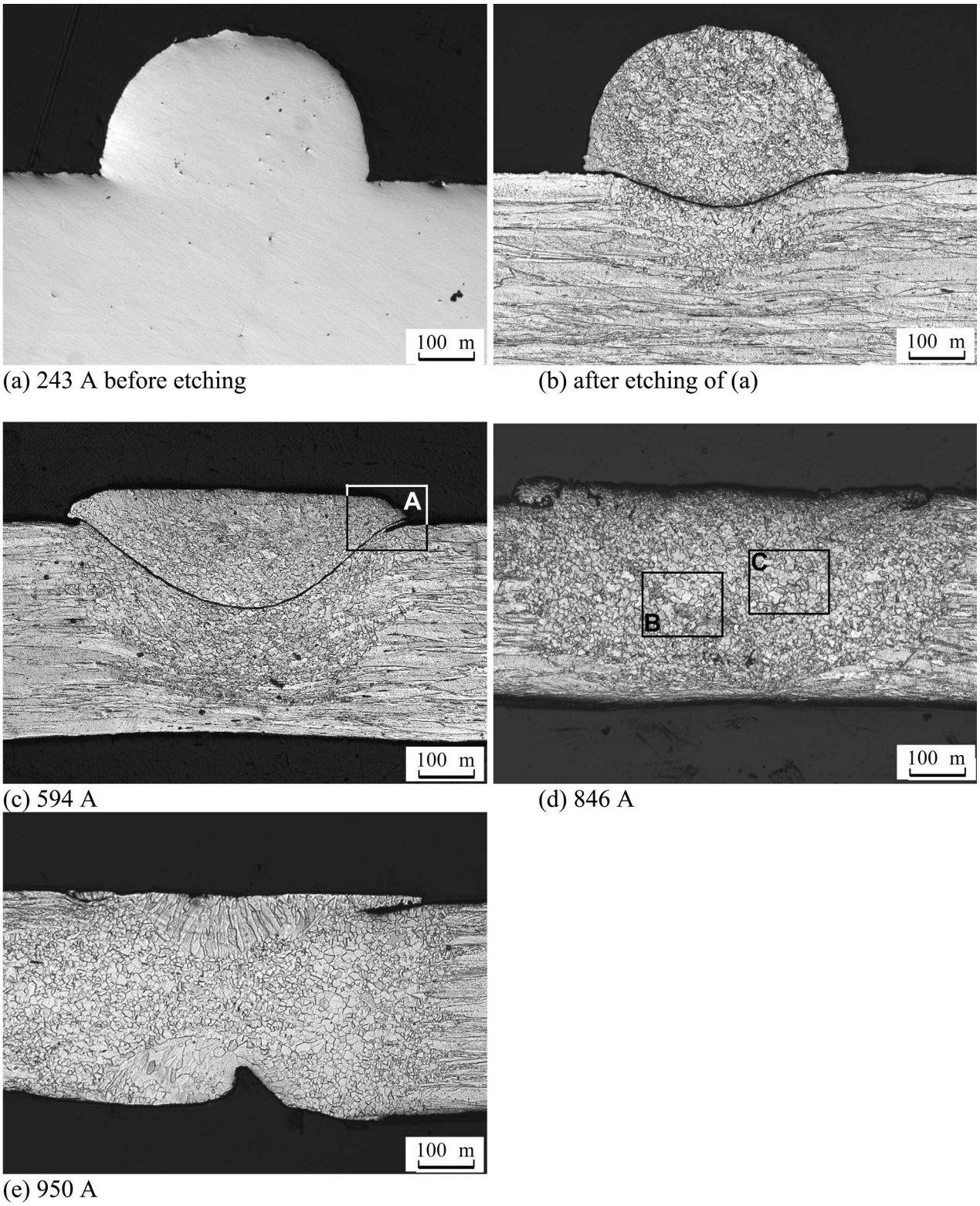

Fig. 4—Cross sections of joints made at different welding currents, with welding force of 6 kg and weld time of six cycles: (*a*) 243 A before etching, (*b*) after etching of (a), (*c*) 594 A, (*d*) 846 A, and (*e*) 950 A.

weld time. However, both joint breaking force and setdown continued to increase until about three cycles. Most joints fractured through the bond interface when the current was below 483 A (Figure 8(a)). Some of the joints made at a current of 483 A when the weld time was above six cycles, and the all joints made at a current of 594 A, fractured in the HAZ. Figure 6 appears to confirm again, as compared to Figure 8, that the parameter of setdown was important in determining

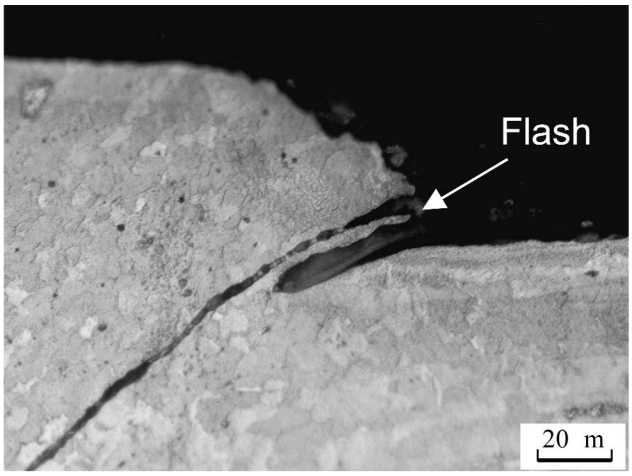

area A

(*a*)

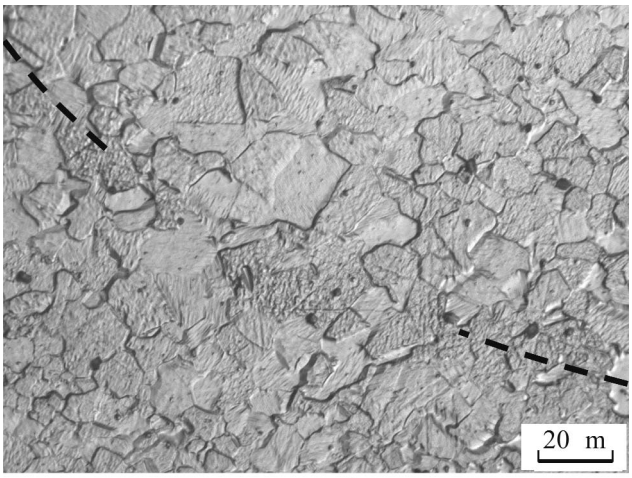

area B

(*b*)

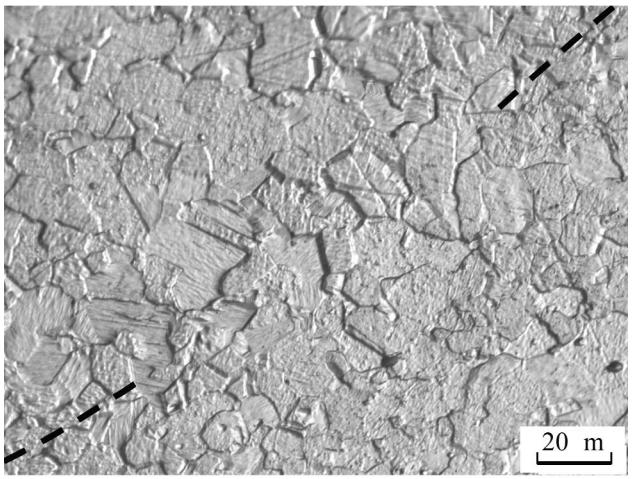

area C

(*c*)

Fig. 5—Details of highlighted areas in Fig. 4: (*a*) area A, (*b*) area B, and (*c*) area C.

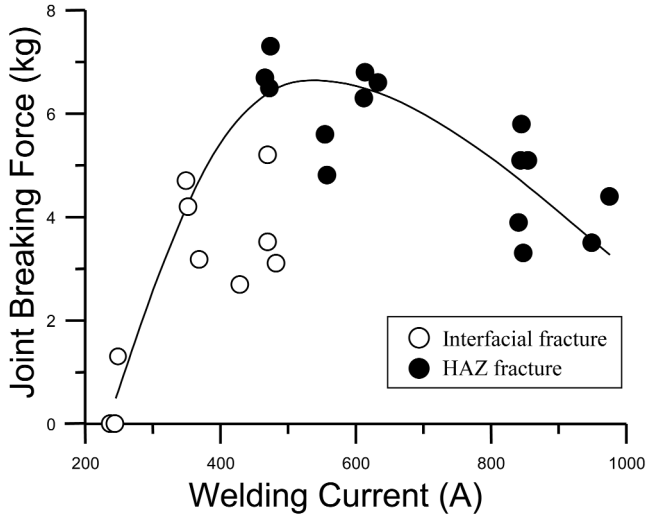

(*a*)

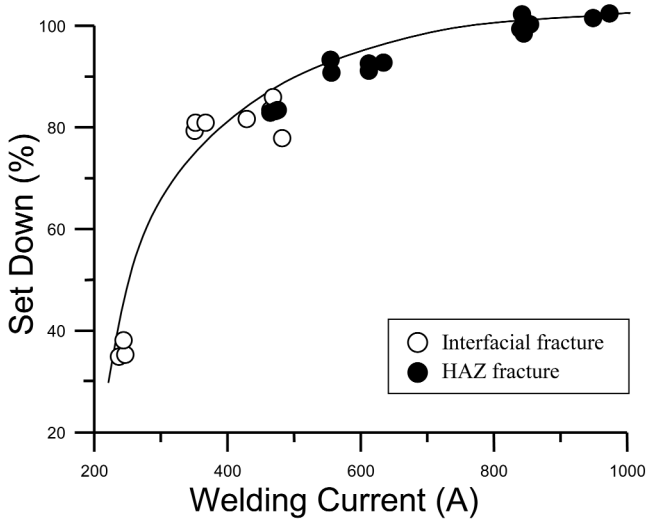

(*b*)

Fig. 6—Effects of welding current on (*a*) joint breaking force and (*b*) setdown.

joint strength before the joint strength reached its maximum, as also suggested by previous work.[3,8]

Some joints were quenched into water immediately after welding to investigate the effect of natural cooling on the evolution of microstructure. The recrystallization structure was still identified in water-quenched joints made at the shortest weld time. This implies that the recrystallized microstructure was developed during the welding sequence, *i.e.*, as dynamic recrystallization. During the holding and air-cooling, static recrystallization continued, resulting in only slight additional grain growth with the formation of annealing twins.

C. *Effect of Welding Force*

Figure 9 shows a typical indentation on a wire from a cross-wire assembly that was subjected only to welding force but no current, which would be close to the initial contact area. The size and contact conditions of this initial contact area, as determined by the welding force, wire hardness, and surface condition,

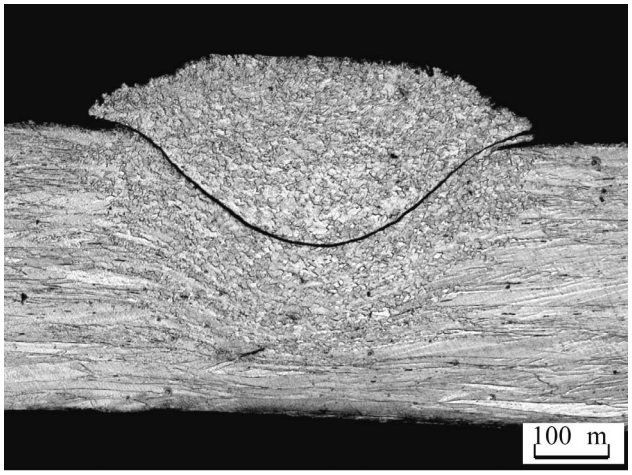

1 cycle

(*a*)

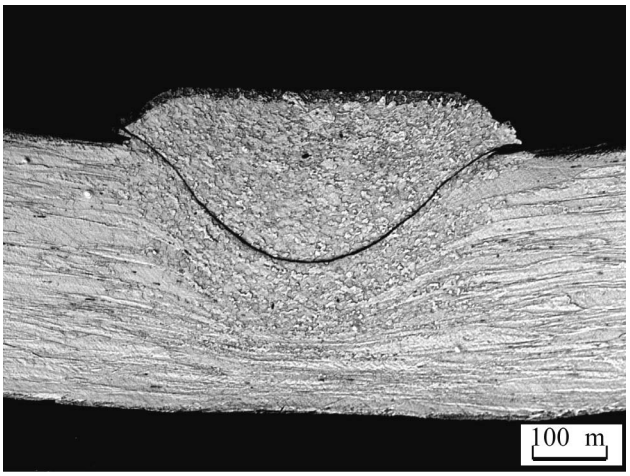

3 cycles

(*b*)

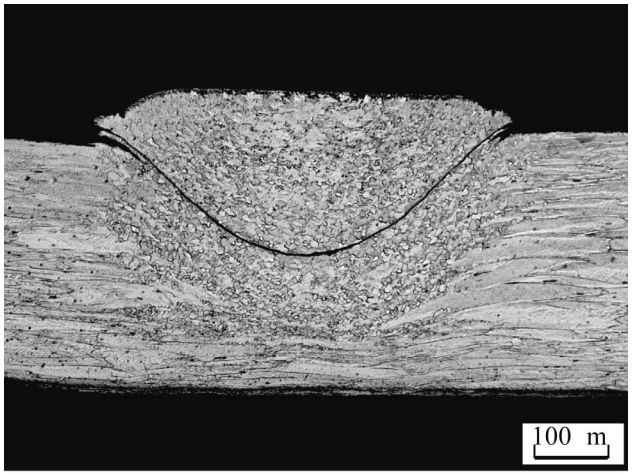

12 cycles

(*c*)

Fig. 7—Cross sections of joints made at different welding times, with welding current of 483 A and welding force of 6 kg: (*a*) 1 cycle, (*b*) 3 cycles, and (*c*) 12 cycles.

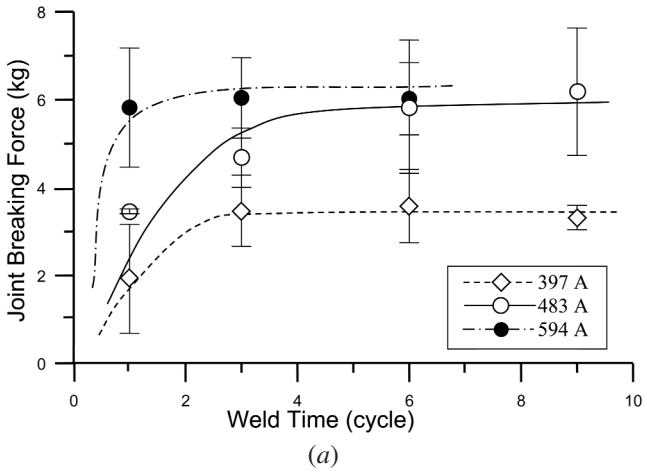

(*a*)

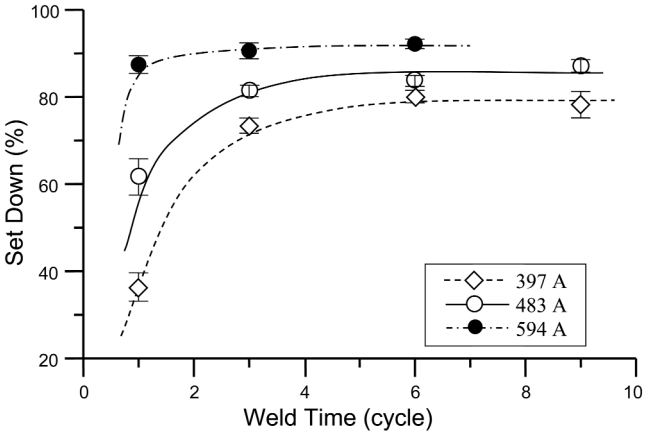

(*b*)

Fig. 8—Effects of weld time on (*a*) joint breaking force and (*b*) setdown at different welding currents.

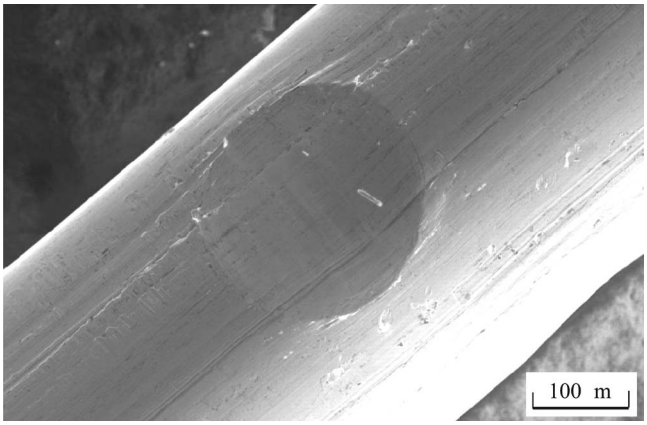

Fig. 9—Indentation on nickel wire with welding force of 6 kg without current.

would affect the initial contact resistance.[7] A greatly increased contact area during welding (comparing Figures 9 to 4) would cause a sharp drop in contact resistance, which implies that, with such a special joint geometry in this work, the initial contact resistance would play a major role in determining heat generation (Eq. [1]). This was confirmed by the experimental observation, in which the microstructure did not change much

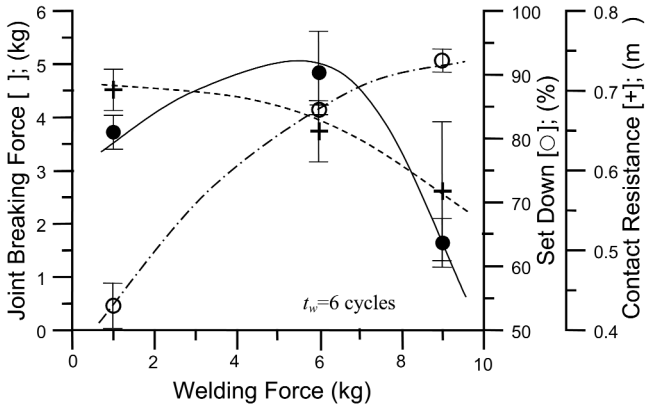

Fig. 10—Effects of welding force on joint breaking force, setdown, and initial contact resistance between wires.

after the first cycle (Figure 7). Therefore, the initial contact resistance was also investigated experimentally.

Figure 10 shows the relation between joint breaking force, setdown, and initial contact resistance between wires, in which all the joints fractured at the bond interface in tensile-shear testing. As the welding force increased, the initial contact resistance decreased and setdown increased, both as expected. But, there appeared to be an optimum welding force in terms of joint breaking force. Furthermore, Figure 10 appears to indicate that an increased setdown would not necessarily result in a higher joint breaking force when interfacial failure occurs. This is opposite to the trends observed in Figures 6 and 8 and in the literature.[3,8] In other words, setdown, as an indication of wire deformation, may not be a sufficient predictor of joint strength. Possible reasons for the optimum in welding force in Figure 10 will be discussed later.

IV. DISCUSSION

A. *Bonding Mechanism*

Depending on joining processes employed (fusion welding, brazing/soldering, and solid-state bonding), roughly three approaches are used to eliminate surface contamination (mainly oxide films), which is the greatest single impediment to metallurgical bonding between two metallic surfaces.[10,11,12] One is the use of a chemical flux, which removes oxide films from surfaces being joined (as in brazing and soldering): this is irrelevant in this work, since no fluxes were used. Another approach is by melting and/or washing away of oxide films, as in fusion welding, when the adjacent base metal becomes molten. The last, as in solid-state bonding processes, is by breaking up oxide films by mechanical means (*e.g.*, surface extension due to plastic flow, as in pressure welding). The last two (*i.e.*, melting and plastic flow) are possible in this work, since both resistance heating and electrode force (pressure) are available. The present work suggests that resistance microwelding of crossed fine nickel wires is a mixture of effects in which the joint is formed mainly by solid-state bonding, but with a transient molten film at the faying interface, similar to some other resistance welding processes (such as flash welding, high-frequency welding, and, possibly, projection welding[10]), such that thin films of molten metal are formed at faying surfaces and subsequently squeezed out by forging force.

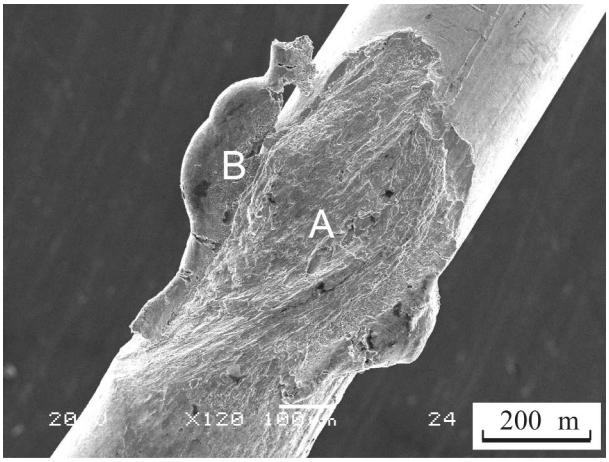

(*a*) Fractured surface

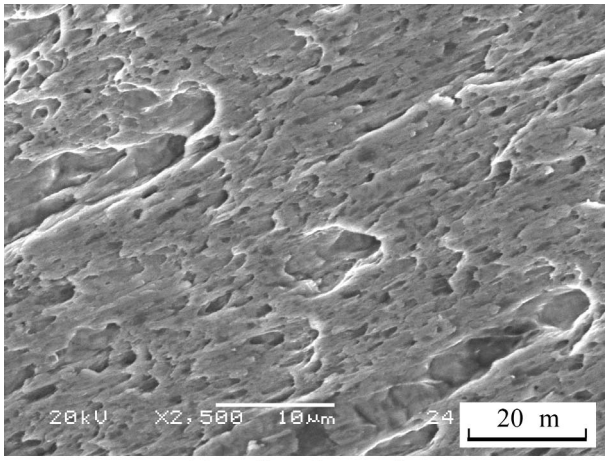

(*b*) Details of area A

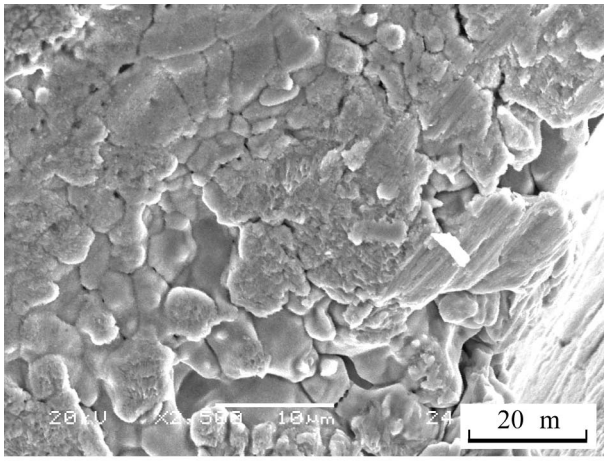

(*c*) Details of area B

Fig. 11—Fractured surface of a joint made at welding force of 1 kg, welding current of 355 A, and weld time of nine cycles: (*a*) fractured surface, (*b*) details of area A, and (*c*) details of area B.

Detailed SEM/EDX analysis was performed on the flashes formed at the edge of the bond interfaces (Figures 4 and 7). The results, showing a solidification structure and high levels of impurities (Figures 11(a) and (c) and Figure 12(b), as compared to Figure 1), suggested that the flash comprised traces

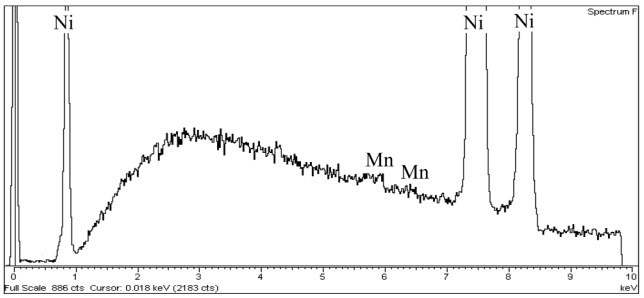

(*a*)

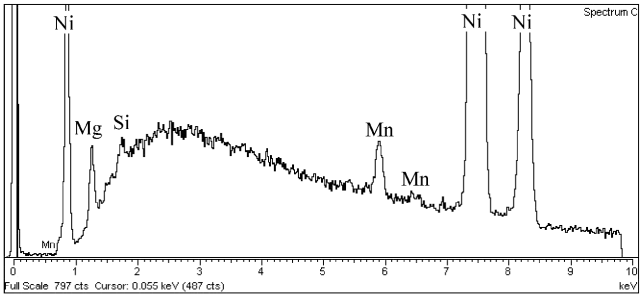

(*b*)

Fig. 12—EDX analyses of area A and B in Fig. 11: (*a*) area A and (*b*) area B.

of the molten metal squeezed out from the bond interface. This molten metal, containing high levels of impurities because of the surface contamination on the original wire surface (oxides and other impurities, as shown in Figure 2), was squeezed out by the welding force to form the flashes. Relatively clean faying surfaces (Figure 9(d)) were, thus, created to form metallurgically sound bond interfaces during welding, as indicated by the ductile-shear fractured surface (Figure 11(b)). Elimination of surface oxide films by solid-state plastic flow was not observed in this work, which appears to be consistent with the experimental observations that nickel is among the most difficult metals to be pressure welded.[12]

Therefore, based on the previous results and discussion, a process sequence of resistance cross-wire microwelding of fine nickel wires is proposed, as shown in Figure 10. An indentation between crossed wires would occur in stage 1 (Figure 9), since point contact between the wires would deform when subjected to the electrode force. After the current is turned on, surface melting occurs at the contact area (stage 2 in Figure 13) because of the high initial contact resistance (and, hence, heat generation). Dynamic recrystallization would occur near the bond interface as the temperature filed builds up around the interface. The molten phase would be almost immediately squeezed out, carrying some of the surface contaminants/impurities as the wires rapidly collapsed at the elevated temperature, resulting in relatively clean faying surfaces for metallurgical bonding (stage 3 in Figure 13). The first three stages would be completed within the first couple of cycles. The wires would continue to collapse/deform due to the combined effect of elevated temperature and electrode force (stage 4 in Figure 13), but the heat generation would be greatly reduced, since most of the contact resistance at the faying interface would disappear due to expansion and cleaning of the faying surface, and any further heat generation would come mainly from the bulk resistance. The bond interface would ultimately disappear as new grains grow across the interface as a result of dynamic recrystallization and, probably, also as remaining impurities diffuse away. After stage 4, the current is turned off and the temperature may still be high enough to promote static recrystallization with annealing twins forming near the interface. Electrode force serves also as the forging force in stage 4. Therefore, resistance cross-wire microwelding of fine nickel wires is basically a solid-state joining process with transient surface melting at the early stage of the process. It is believed that sufficient surface melting and subsequent squeezing out of this transient molten phase is a prerequisite for strong solid-state bonding.

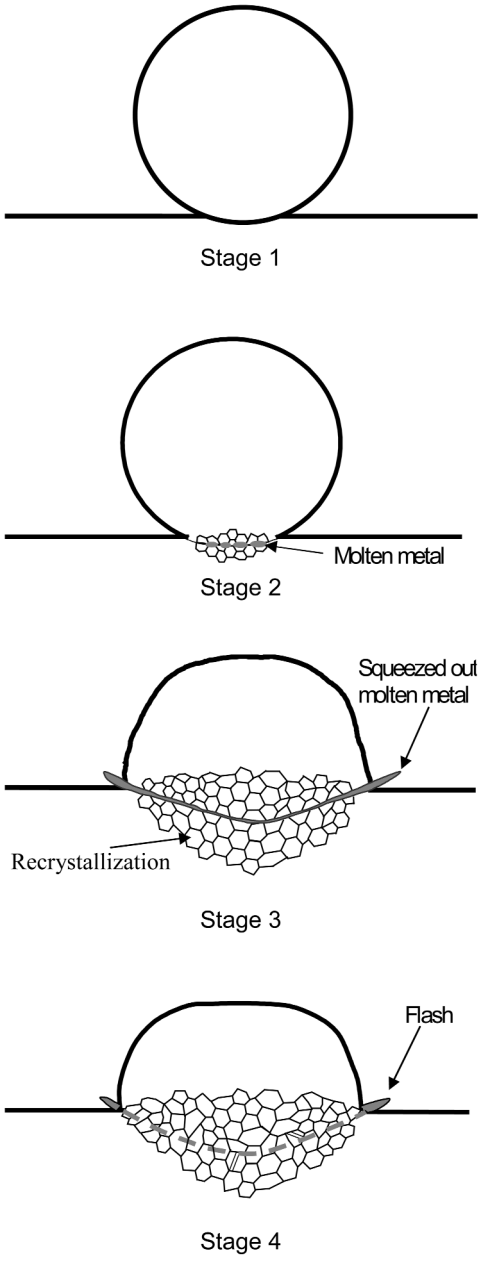

Fig. 13—Main stages in resistance microwelding of crossed fine nickel wires.

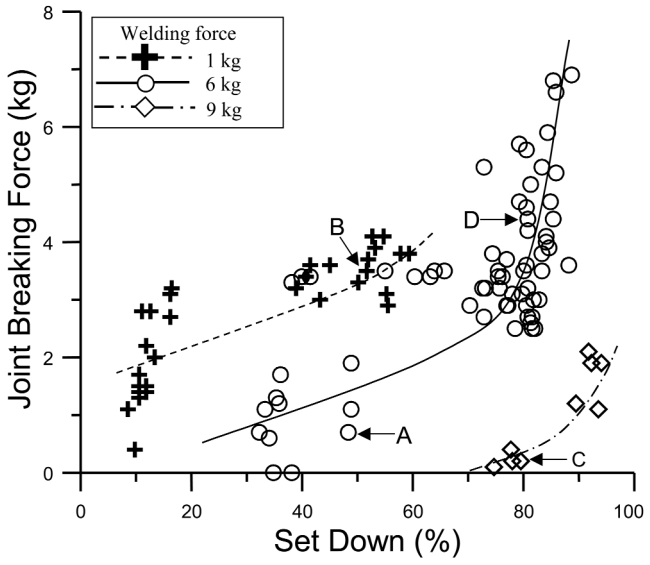

Fig. 14—Joint breaking force *vs* setdown, with welding force indicated in the legend.

B. *Process Optimization*

As observed in Section III–C, setdown may not be a sufficient criteria to be used to evaluate joint strength, which disagrees with some previous observations,[3,8] even when only interfacial failure occurred. To further study the relation between joint strength and setdown, all the mechanical-test results at different welding conditions but with interfacial failures are plotted in Figure 14 (*i.e.*, each data point was at a different weld time, welding current, and force). It is interesting to note that the data could be roughly separated into groups according to welding force, in which, at each welding force, joint strength (indicated by the joint breaking force) increased with increasing of setdown as a result of combined changes in welding current and weld time. But, this is not true when groups welded with different welding forces were compared.

Two data points (A and B in Figure 14) with similar setdowns were selected to investigate why the strength values were so different. A granular fracture surface (Figure 15(b)), similar to the solidification microstructure in Figure 11(c), was observed with the weak bond interface, while a ductile

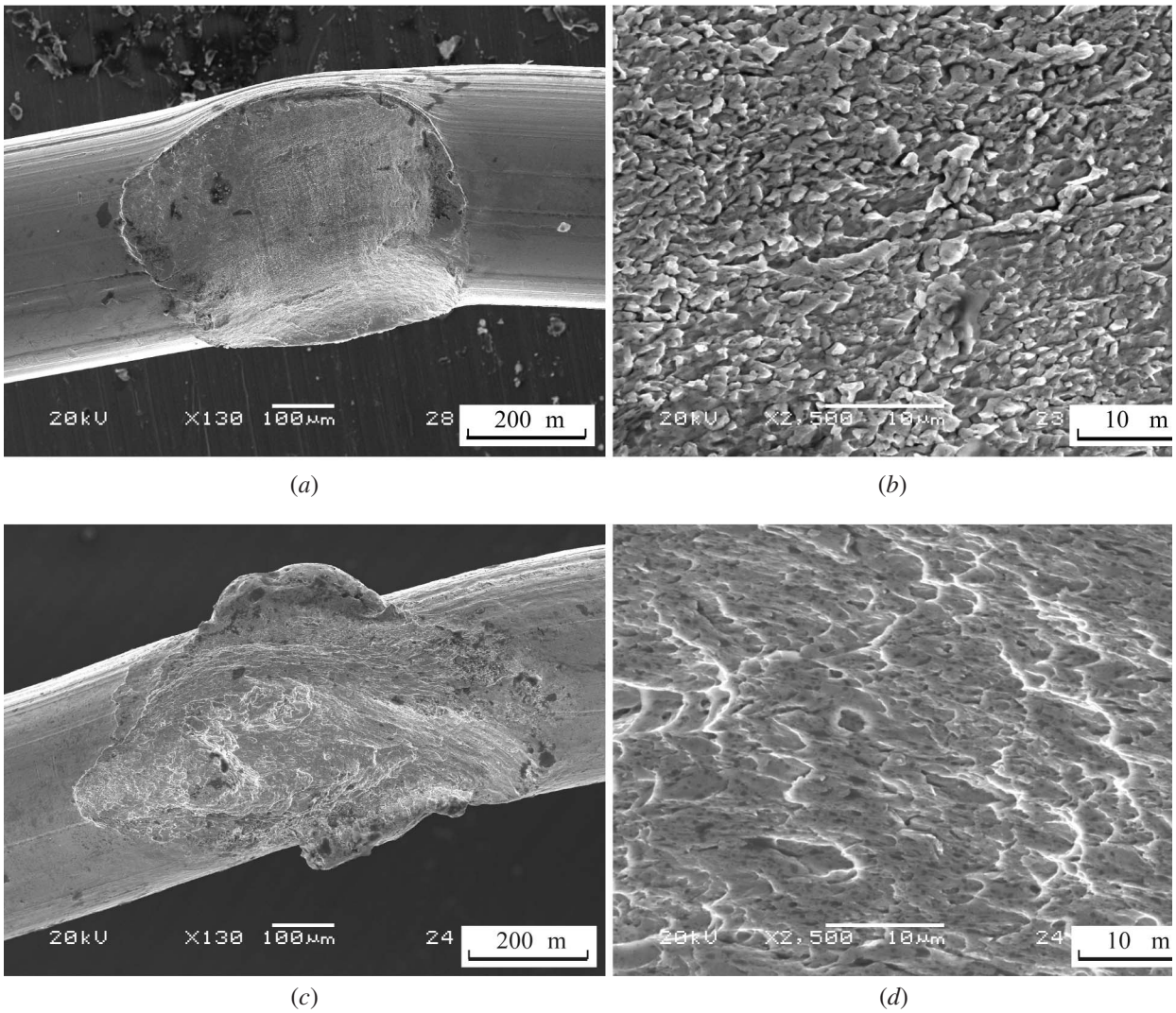

Fig. 15—Fractured surfaces of joints A and B in Fig. 14. (*a*) Joint A (at welding current of 231 A, welding force of 6 kg, weld time of six cycles, and setdown of 48 pct). (*b*) Details of the center in (a). (*c*) Joint B (at welding current of 237 A, welding force of 1 kg, weld time of six cycles, and setdown of 52 pct). (*d*) Details of the center in (c).

fracture surface (Figure 15(d)) was associated with the strong bond interface. The EDX analysis confirmed the relatively high level of impurities (as in Figure 12(b)) and low impurities (as in Figure 12(a)) on the fracture surfaces in Figures 15(b) and (d), respectively. Therefore, it is postulated that a low initial contact resistance and, hence, heat generation due to the higher welding force in the case of point A in Figure 15 would produce only limited surface melting and, at least, part of the molten phase produced would be trapped between the faying surfaces, resulting in a weak bond. The setdown in this case was mainly achieved by "cold" deformation/collapse. In case B of Figure 15, the lower welding force would result in a high initial contact resistance and, hence, heat generation, which would form sufficient molten phase to be squeezed out to produce relatively "clean" surfaces for bonding. In this situation, the wire deformation, which helped to squeeze out the surface melting, was achieved by rapid temperature buildup even though the welding force was relatively low (hereafter referred as "hot" deformation/collapse). In other words, since the joint strength, as indicated by joint breaking force, is really determined by the product of the bonded area and bond interfacial strength, the interfacial strength was quite different in the cases of points A and B in Figure 14, although both had similar bonded areas (as measured by the setdown). The difference between cold and "hot" collapse could be further demonstrated by the data points C and D in Figure 14, both with similar setdowns (Figure 16). A recrystallized microstructure was associated with a strong bond interface (Figure 16(b)), while a cold-pressed microstructure with little recrystallization was associated with a weak bond interface (Figure 16(a)). Therefore, not only a sufficient setdown, but also an appropriate local temperature history associated with this setdown is important to produce a strong bond interface.

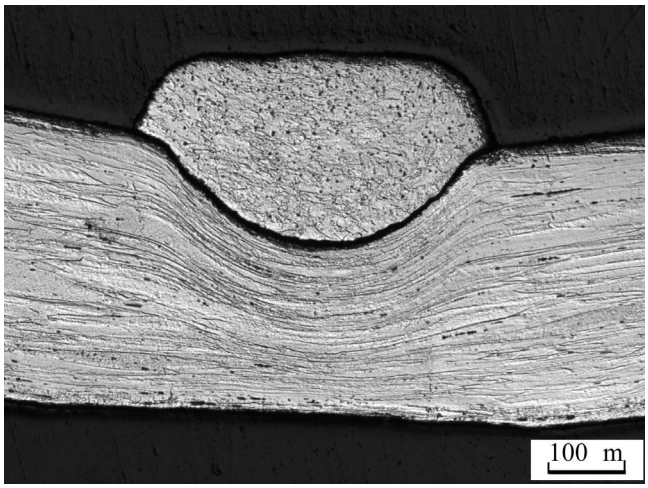

(*a*)

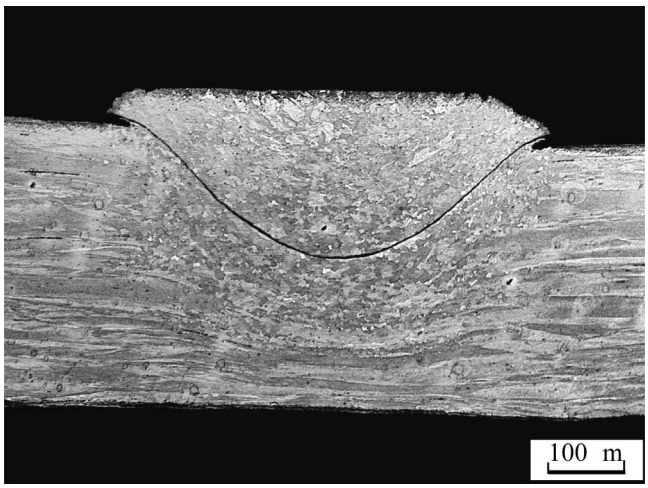

(*b*)

Fig. 16—Cross sections of joints C and D in Fig. 14. (*a*) Joint C (at welding current of 316 A, welding force of 9 kg, weld time of six cycles, and setdown of 78 pct). (*b*) Joint D (at welding current of 408 A, welding force of 6 kg, weld time of six cycles, and setdown of 84%).

With the concepts of cold and hot collapse, the existence of an optimum in welding force in Figure 10 could be easily understood. An increase in welding force, if it did not affect heat generation too much, would increase the bonded area, resulting in an increase of the joint breaking force (hot collapse). However, a further increase in welding force would reduce heat generation too much to achieve high interfacial strength, resulting in a low joint breaking force, even though a relatively large wire deformation was achieved (cold collapse).

Therefore, optimized process parameters need to produce sufficient surface melting at the very beginning of the welding sequence. This molten metal, carrying the surface contamination, needs to be squeezed out to produce "clean" surfaces for a strong bond. A relatively large bonded area is also required, since the load-carrying capacity of the joint is determined by both interfacial strength and bonded area. Either a high welding current or low welding force seems to be effective to produce sufficient molten phase. However, too high a welding current would cause electrode sticking and degrade the wire properties in the HAZ, and too low a welding force cannot produce a sufficiently large bonded area. On the other hand, although a large welding force can increase the bonded area, it would also reduce the initial contact resistance and, hence, heat generation, which produces insufficient surface melting.

The ideal situation would be to use a lower electrode force at the beginning of welding to obtain sufficient heat generation and, successively, to increase the force to obtain a large bonded area. This idea was tested as shown in Table II, in which the effect of firing force on joint strength was evaluated. The welding apparatus used in this work takes several mini-

Table II. Effects of Firing Force on Joint Breaking Force

Firing Force (kg)	Welding Current (A)	Joint Breaking Force (kg)	Set Down (Pct)	Fracture Mode
1.0	347 ± 62	5.8 ± 0.4	74 ± 3	interfacial (two samples), HAZ (three samples)
5.8	396 ± 58	3.6 ± 0.8	80 ± 1	interfacial (five samples)

Note: welding force = 6.0 kg; weld time = six cycles.

seconds to build up the electrode force from zero to a nominal value, as air flows into the electrode actuator. A relatively low firing force, that is, initiating the welding current well before the electrode force had increased to its set point, resulted in high heat generation to produce sufficient surface melting, and the larger welding force then worked as a forging force to enlarge the bonded area while squeezing molten metal out. Figure 17 shows the fractured surfaces of those joints. The joint with low firing force showed a ductile dimpled shear morphology on almost all the fracture surfaces. On the other

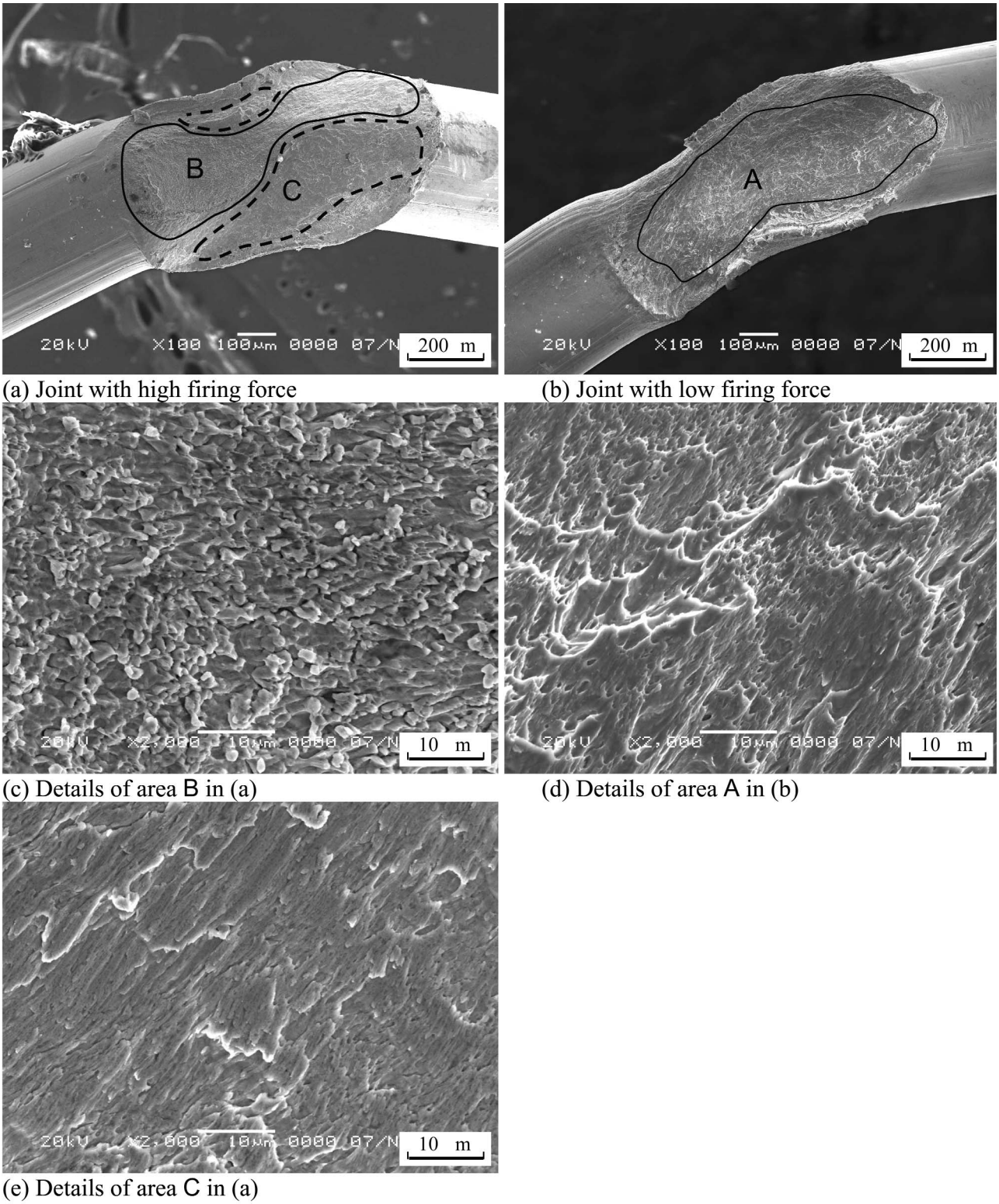

Fig. 17—Fractured surfaces of joints made with (*a*) high firing force of 5.8 kg and (*b*) low firing force of 1 kg. Both joints had welding force of 6 kg. (*a*) Joint with high firing force. (*b*) Joint with low firing force. (*c*) Details of area B in (a). (*d*) Details of area A in (b). (*e*) Details of area C in (a).

hand, the joint with a large firing force indicated a granular and relatively flat shear morphology in the center, while the outer region appeared to be just unbonded, deformed original surfaces. This experimental trial has clearly demonstrated that setting a low firing force relative to the higher welding force could be used to improve both the interfacial strength and bonded area. This differs significantly from the general industry practice where firing force (point of current initiation) is usually set at 90 to 97 pct of the full welding force.

V. CONCLUSIONS

Resistance microwelding of crossed fine nickel wires was investigated by means of detailed mechanical testing and metallurgical examinations. The main conclusions include the following.

1. The welding current and force had the greatest effects on joint microstructure evolution and, hence, joint strength, compared to weld time. Increasing the welding current increased the joint breaking force, but too high a current caused a lower breaking force because of recrystallization softening in the HAZ. An optimum welding force was observed, with a low welding force resulting in a low joint breaking force because of the low bonded area and excessive welding force reducing the breaking force because of low interfacial strength
2. It is proposed that resistance microwelding of crossed fine nickel wires includes the following stages: (1) cold-wire collapse, (2) surface melting, (3) molten-phase squeeze out, and (4) solid-state bonding. it is believed that sufficient surface melting and subsequent squeezing out of the molten phase is needed to produce fresh metal surfaces for strong solid-state bonding.
3. Sufficient local heat generation is the key to high-quality welds, first, to generate sufficient surface melting and, second, to facilitate plastic deformation (measured as set-down) in order to squeeze out the molten metal and expand the bonded area. This requires a proper balance of high initial contact resistance and sufficiently high welding force, which could be easily realized by setting a low firing force compared to the nominal welding force.

ACKNOWLEDGMENTS

This work has been supported by the Canada Research Chairs Program (www.crc.gc.ca). Experimental assistance from Mr. K. Chan, University of Waterloo, in this study is greatly appreciated.

REFERENCES

1. *Resistance Welder Manufactures' Association (RWMA): Resistance Welding Manual*, 4th ed., George H. Buchanan Co., Philadelphia, PA, 1989, Sec. 1.
2. V.E. Ataush, E.G. Moskvin, and V.P. Leonov: *Weld. Int*., 1992, vol. 6 (8), pp. 624-27.
3. V.I. Stroev, V.E. Ataush, and Y.A. Rudzit: *Weld. Int*., 2000, vol. 14 (6), pp. 491-95.
4. K.J. Ely and Y. Zhou: *Sci. Technol. Welding Joining*, 2001, vol. 6 (2), pp. 63-72.
5. Y. Zhou, S.J. Dong, and K.J. Ely: *IEEE/TMS J. Electron. Mater*., 2001, vol. 30 (8), pp. 1012-20.
6. Y. Zhou, P. Gorman, W. Tan, and K.J. Ely: *IEEE/TMS J. Electron. Mater*., 2000, vol. 29 (9), pp. 1090-99.
7. B.H. Chang, M.V. Li, and Y. Zhou: *Sci. Technol. Welding Joining*, 2001, vol. 6 (5), pp. 273-80.
8. V.E. Moravskii, V.N. Korzh, and S.P. Svidergol: *Automatic Welding*, 1980, vol. 33 (9), pp. 24-26.
9. D. Baber, D.C. Koehler, W.O. Fleckenstein, G.E. Roden, and R. Sakia: *Physical Design of Electronic System*, vol. III, *Integrated Device and Connection Technology*, Prentice-Hall, Inc., Englewood Cliffs, NJ, p. 439.
10. *Welding Handbook*, vol. 2, *Welding Processes*, 8th ed., American Welding Society, Miami, FL, 1991, p. 581.
11. W. Tan, Y. Zhou, and H.W. Kerr: *Metall. Mater. Trans. A*, 2002, vol. 33A, pp. 2667-76.
12. D.R. Milner and G.W. Rowe: *Metall. Rev*., 1962, vol. 7 (28), pp. 433-80.